Journal of Marine Systems 224 (2021) 103634

Contents lists available at ScienceDirect

Journal of Marine Systems

journal homepage: www.elsevier.com/locate/jmarsys

Biological carbon pump efficiency enhanced by atmospheric dust deposition in the North Pacific Subtropical Gyre

Hyung Jeek Kim [a], Dongseon Kim [b], Chan Min Yoo [c], Jong-Yeon Park [d], Hyeryeong Jeong [b], Jeomshik Hwang [e,*]

[a] Jeju Marine Research Center, Korea Institute of Ocean Science & Technology, Jeju, Republic of Korea
[b] Marine Environmental Research Center, Korea Institute of Ocean Science & Technology, Busan, Republic of Korea
[c] Deep-sea Mineral Resources Research Center, Korea Institute of Ocean Science & Technology, Busan, Republic of Korea
[d] Department of Earth and Environmental Sciences, Chonbuk National University, Jeonju, Republic of Korea
[e] School of Earth and Environmental Sciences/Research Institute of Oceanography, Seoul National University, Seoul, Republic of Korea

ARTICLE INFO

Keywords:
Atmospheric dust deposition
Sediment trap
Particle flux
Biological pump
North Pacific Subtropical Gyre

ABSTRACT

We examine the flux and composition of sinking particles collected at 4500 m depth in the southeastern part of the North Pacific Subtropical Gyre (NPSG) from August 2011 to June 2012. Satellite-derived net primary production was higher in January–May 2012 compared with the rest of the study period. Both the biogenic and lithogenic particle fluxes were significantly higher in spring (March–May 2012) than at other times. The export efficiency via the transfer of produced organic carbon to the deep ocean interior (i.e., carbon sequestration) doubled during this time. Two prominent particle flux peaks were observed in March and May 2012, coinciding with the atmospheric dust-deposition peaks within the temporal resolution of the data. Coincident increases in the biogenic and lithogenic particle fluxes suggest that dust deposition in the NPSG enhances the biological carbon-pump efficiency. Strong coupling between the particulate organic carbon and biogenic opal fluxes implies that nutrient supply via atmospheric dust deposition stimulated diatom growth in this area. Dust deposition during the productive season therefore plays an important role in carbon sequestration.

1. Introduction

The surface water of the North Pacific Subtropical Gyre (NPSG; spanning approximately 15°–35°N and 135°E–135°W) is characterized by low nitrate (NO_3^- < 5 nM in the upper 100 m) and chlorophyll-*a* concentrations (Karl, 1999; Dore et al., 2008; Karl and Letelier, 2008). The remoteness of this large ecosystem has resulted in limited direct sampling (Karl, 1999). The Hawaii Ocean Time-series (HOT) research program has extensively advanced our understanding of the biogeochemical processes and particle export in the pelagic zone of the NPSG (Karl and Church, 2017), but particle transport to the deep bathypelagic environment of the NPSG remains poorly understood.

East Asian dust (EAD) from the deserts in northern China and Mongolia is transported to the North Pacific mainly in spring via the prevailing westerlies within several days of dust development (Johnson et al., 2003; Yuan and Zhang, 2006; Lee et al., 2015). EAD deposition provides essential nutrients (Tan et al., 2013; Yoon et al., 2017) and stimulates primary production (Li et al., 2004; Calil et al., 2011; Tan et al., 2013; Martino et al., 2014; Letelier et al., 2019). The phytoplankton community in the NPSG is sensitive to the nutrient supply via EAD deposition (White et al., 2007). Natural iron (Fe) fertilization via EAD deposition in the NPSG has been suggested to be a stimulant for phytoplankton growth (Calil et al., 2011), as was the case for the subarctic North Pacific, which is a high-nutrient, low-chlorophyll region (Harrison et al., 1999; Bishop et al., 2002). Yoon et al. (2017) analyzed regional satellite observations in the western North Pacific, and reported that EAD deposition can increase primary production by more than 70% compared with non-dust conditions.

The impact of EAD deposition on biogeochemical processes, such as nutrient supply and net primary production (NPP), has been investigated at Station ALOHA (A Long-term Oligotrophic Habitat Assessment) (e.g., Letelier et al., 2019). However, the impact of EAD deposition on

* Corresponding author at: School of Earth and Environmental Sciences/Research Institute of Oceanography, Seoul National University, Seoul 08826, Republic of Korea.
E-mail addresses: juac29@kiost.ac.kr (H.J. Kim), dkim@kiost.ac.kr (D. Kim), cmyoo@kiost.ac.kr (C.M. Yoo), jongyeon.park@jbnu.ac.kr (J.-Y. Park), hrjeong@kiost.ac.kr (H. Jeong), jeomshik@snu.ac.kr (J. Hwang).

https://doi.org/10.1016/j.jmarsys.2021.103634
Received 3 May 2021; Received in revised form 18 August 2021; Accepted 25 August 2021
Available online 1 September 2021

the efficiency of the biological-pump (i.e., transport of organic carbon from surface water to the deep ocean) has not been well reported. Direct measurements of the sinking flux of biogenic particles via sediment traps can further advance our understanding of biological-pump response to atmospheric dust deposition and the associated nutrient supply. Most investigations of the atmospheric dust input to the deep sea have been conducted in the Atlantic (Brust and Waniek, 2010; Brust et al., 2011). The effect of Saharan dust deposition in the northern subtropical gyre was investigated for comparison with its southern counterpart, where there is no obvious dust supply (Pabortsava et al., 2017). Saharan dust deposition enhanced both primary production and biological-pump efficiency through nutrient supply and mineral ballast (Pabortsava et al., 2017). Bishop et al. (2002) found that EAD deposition increased the export efficiency of particulate organic carbon (POC) to the deep ocean using data from Argo-type floats deployed near Station PAPA in the subarctic North Pacific.

We measured the flux and composition of sinking particles collected for a year at 4500 m depth in the southeastern edge of the NPSG (Fig. 1). We investigated the biological pump in the NPSG based on the particle flux data and satellite-derived NPP, with the special focus on the role of atmospheric deposition.

2. Material and methods

The Korea Institute of Ocean Science and Technology (KIOST) occupied a site near the southeastern edge of the NPSG, Station KOMO2 (16.5°N, 131.0°W), to investigate particle transport to the deep ocean interior (Fig. 1). This site is located ~660 km north of Station KOMO1 (10.5°N, 131.2°W), where the particle flux at 4950 m depth was monitored for ~10 years from 2003 to 2013 (Kim et al., 2019). A time-series sediment trap (PARFLUX Mark 78H 21-sample bottles; McLane Research Labs, USA) was deployed at 4500 m depth (500 m above the seafloor) at Station KOMO2 from August 2011 to June 2012. The sediment trap was attached to wire mooring pennants with type 316 stainless steel shackles to prevent extraneous metal and organic contamination during the deployment period. Sinking particles were collected weekly for March–May 2012 and monthly for the remainder of the study period (Table 1). Sample bottles were filled with filtered seawater that was collected from the sediment trap deployment depth. Formalin solution (5%) buffered with sodium-borate was added to the filtered seawater as a preservative. Upon sediment trap recovery, the sampling cups were capped and stored at 4 °C in a refrigerator until analysis. Samples were processed within a month.

Swimmers larger than 1 mm were separated from the particles by hand in the laboratory. Each sample was split into five equal aliquots using a wet-sample divider (WSD-10; McLane Research Labs, USA). This type of sample divider is known to have precision better than 3.7% (Honjo and Manganini, 1993; Honjo et al., 1995). The three aliquots of each sample were combined into a single sample. The sample was centrifuged after rinsing with Milli-Q water to remove salts and any residual formalin solution. The centrifuged samples were then freeze-dried and weighed for gravimetric determination of the total particle flux. The dried samples were homogenized in an agate mortar and used for total carbon (TC), total inorganic carbon (TIC), and biogenic silicon (bSi) content analysis. The TC content of each sample was analyzed using a Flash EA1112 NC analyzer (Thermo Fischer Scientific, USA), with the precision of the analysis (relative standard deviation) smaller than 0.7% based on multiple analysis of a standard material (sulfanilamide, CE instruments). The TIC content was measured using a UIC CO_2 coulometer (CM 5014; UIC Inc., USA), with an analysis error of 0.2% based on multiple analysis of a standard material (calcium carbonate, Sigma Aldrich). The calcium carbonate ($CaCO_3$) content was calculated by multiplying the TIC content by 8.33 (Trapote et al., 2018). The POC content was estimated as the difference between TC and TIC contents. The wet-alkaline extraction method of Kim et al. (2011), modified from Mortlock and Froelich (1989) and Müller and Schneider (1993), was used to determine the bSi content. The biogenic opal content was calculated by multiplying the bSi content by 2.4 (Lee et al., 2003). The precision of bSi analyses was better than 2% relative standard deviation, based on duplicate analyses of 5 samples.

For foraminiferal flux analysis, an aliquot of each sample was wet-sieved through a 63-μm mesh and then freeze-dried. Foraminifera were hand-separated using a brush under a stereomicroscope (Zeiss Stemi SV 11; Carl Zeiss Microscopy GmbH, Germany), and weighed to determine the foraminiferal flux (Kim et al., 2012).

For metal analysis, approximately 50 mg of each dried sample was dissolved in a 4:4:1 mixture of HF, HNO_3, and $HClO_4$ on a hot plate at 180 °C for 24 h for total digestion, and then further diluted with 2% nitric acid (German et al., 2002). The aluminum (Al) and Fe concentrations were determined using inductively coupled plasma–mass spectrometry (ICP–MS; ICAP Q, Thermo Fischer Scientific, Germany). A certified reference material (MESS-4; marine sediment, National Research Council Canada) was analyzed four times to verify the accuracy of the metal analysis. Analytical recovery was 97.3% for Fe and

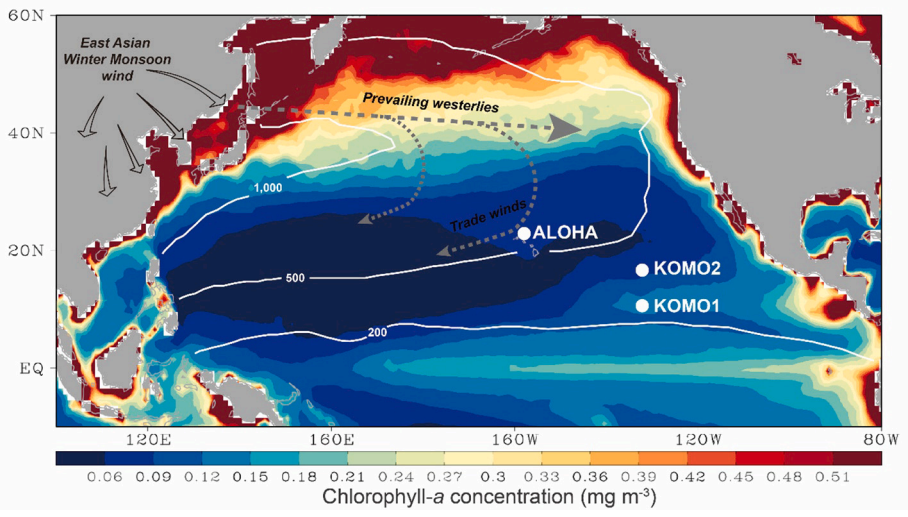

Fig. 1. Map showing the location of Station KOMO2 in the oligotrophic North Pacific Subtropical Gyre. The color shading shows the 2011–2016 average chlorophyll-*a* concentration. The white solid contours indicate the amount of atmospheric dust deposition to the ocean in mg m^{-2} yr^{-1} (Duce, 2014). The dashed lines and arrows indicate the directions of the prevailing westerlies and trade winds in spring (Seo et al., 2014).

Table 1
Sinking particle flux at Station KOMO2 from August 2011 to June 2012. All flux values are in mg $m^{-2}d^{-1}$.

Cup open date (dd/mm/yy)	Sampling interval (days)	Total mass flux	POC flux	$CaCO_3$ flux	Biogenicopal flux	POC %	TN %	Al flux	Fe flux	Planktonic foraminiferal flux
05/08/11	27	14.5	0.88	10.2	0.80	6.07	0.89	0.042	0.028	No data
01/09/11	30	16.2	0.89	11.1	1.03	5.46	0.67	0.066	0.043	4.46
01/10/11	31	12.7	0.97	7.51	1.25	7.60	1.03	0.064	0.042	1.40
01/11/11	30	16.1	0.82	11.5	1.56	5.09	0.62	0.058	0.038	3.06
01/12/11	31	10.8	0.83	5.78	0.62	7.69	0.98	0.066	0.047	1.06
01/01/12	31	1.63	0.14	0.85	0.18	8.33	1.09	0.008	0.006	No data
01/02/12	29	24.3	1.06	18.6	1.78	4.34	0.61	0.065	0.052	4.44
01/03/12	7	15.5	0.55	12.4	No data	3.54	0.44	No data	No data	2.53
08/03/12	7	32.7	1.40	26.2	1.33	4.29	0.58	0.064	0.043	4.54
15/03/12	7	55.0	4.95	32.5	5.60	8.98	1.25	0.206	0.132	10.1
22/03/12	7	41.0	4.28	21.6	4.96	10.4	1.44	0.138	0.092	4.88
29/03/12	7	35.4	3.53	19.2	3.07	9.96	1.34	0.147	0.077	1.94
05/04/12	7	29.5	2.74	15.9	3.42	9.27	1.23	0.14	0.09	No data
12/04/12	7	30.1	2.33	16.3	2.80	7.73	1.02	0.188	0.105	No data
19/04/12	7	19.8	1.67	9.73	No data	8.42	1.09	No data	No data	No data
26/04/12	7	26.0	1.96	14.5	3.22	7.54	1.01	0.128	0.081	No data
03/05/12	7	26.0	2.06	13.1	2.78	7.93	1.15	0.134	0.1	0.62
10/05/12	7	49.0	3.86	29.0	4.85	7.88	1.01	0.16	0.103	8.49
17/05/12	15	58.7	4.67	32.5	5.30	7.95	1.02	0.235	0.146	11.4
01/06/12	30	29.8	1.56	19.2	2.18	5.21	0.69	0.191	0.084	4.84

96.9% for Al.

The NPP (8-day temporal resolution) was estimated from the chlorophyll-*a* satellite data and vertically generalized production model (VGPM) of Behrenfeld and Falkowski (1997). The median NPP value in the 1° × 1° grid box that included the study site was used for comparison with particle flux data. Sea surface temperature (SST) data were obtained from the National Oceanic and Atmospheric Administration (NOAA) optimum interpolation SST product (Reynolds et al., 2002), with monthly and 8-day mean SST fields generated using in situ temperature data and satellite-derived SSTs. The SST data are provided at 1° × 1° horizontal resolution, thus we used the value in 1° grid box that includes the sampling site. Wind-speed data were obtained from the National Centers for Environmental Prediction–Department of Energy (NCEP–DOE) Reanalysis 2 product (Kanamitsu et al., 2002). This is an assimilative product with various operational observations assimilated into a physical atmospheric model, leading to globally available and uniformly gridded datasets. The wind-speed data are provided at 1.875° × 1.875° horizontal resolution. The mixed layer depth was obtained from the NCEP Global Ocean Data Assimilation System (GODAS), which has a 1.0° × 0.333° spatial resolution (Behringer and Xue, 2004). The mixed layer depth in this reanalysis product is defined as the depth where the buoyancy difference from the ocean surface is equal to 0.03 cm s^{-2} (Behringer et al., 1998).

The dust deposition flux around the study site (16.0–17.0°N, 130.5–131.5°W) was produced by the Modern-Era Retrospective analysis for Research and Applications, version 2 (MERRA-2; http://giovanni.gsfc.nasa.gov/giovanni/), which is developed and maintained by the NASA Goddard Earth Sciences Data and Information Services Center (GES DISC) (Acker and Leptoukh, 2007). We used the monthly total dust-deposition flux data in our analysis.

Daily regional mean values of the total aerosol optical depth (AOD) at 550 nm were retrieved from the Moderate Resolution Imaging Spectroradiometer MODIS Terra Level-3 (MODIS08-D3) dataset, which is available on the NASA website (http://giovanni.gsfc.nasa.gov/giovanni/; Papadimas et al., 2009). We averaged the 1° × 1° AOD values over a much wider region of the NPSG (12–22°N, 130–138°W) to obtain enough data for daily averaged AOD values across the study site. The uncertainty in AOD of 550 nm (same as that in MERRA-2) is approximately 20% (Randle et al., 2017).

3. Results

The satellite-derived 8-day mean SST values exhibited sinusoidal variations, with the highest value in September 2011 and lowest value in May–June 2012 (Fig. 2). The monthly mixed layer depth also exhibited sinusoidal variation, with the greatest depth observed in March 2012. High wind speed was generally observed from December 2011 to March 2012. The VGPM-derived NPP values varied between 180 and 524 mg C m^{-2} d^{-1} (Fig. 3a), with lower values in August–December 2011 and higher values in January–June 2012.

The total particle flux ranged between 1.6 and 58.7 mg m^{-2} d^{-1}, with a duration-weighted average of 27.3 mg m^{-2} d^{-1} (Fig. 3a). A low and relatively constant flux was observed in August–December 2011. A marked decrease was then observed in January 2012, with generally higher total particle flux observed in February–June 2012. A notable observation is that two high flux events occurred in spring 2012. Similar high-flux events may have been missed because of the lower sampling resolution in August 2011–February 2012 and June 2012: 1 month as

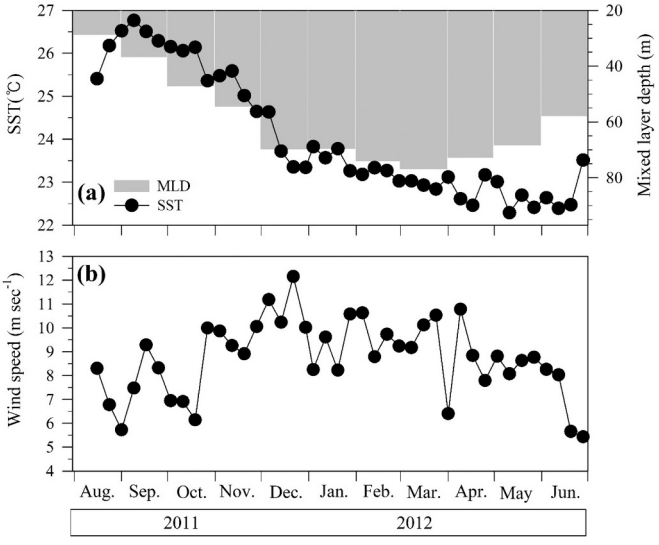

Fig. 2. Temporal variations in (a) sea surface temperature (SST) and mixed layer depth (MLD), and (b) wind speed at Station KOMO2.

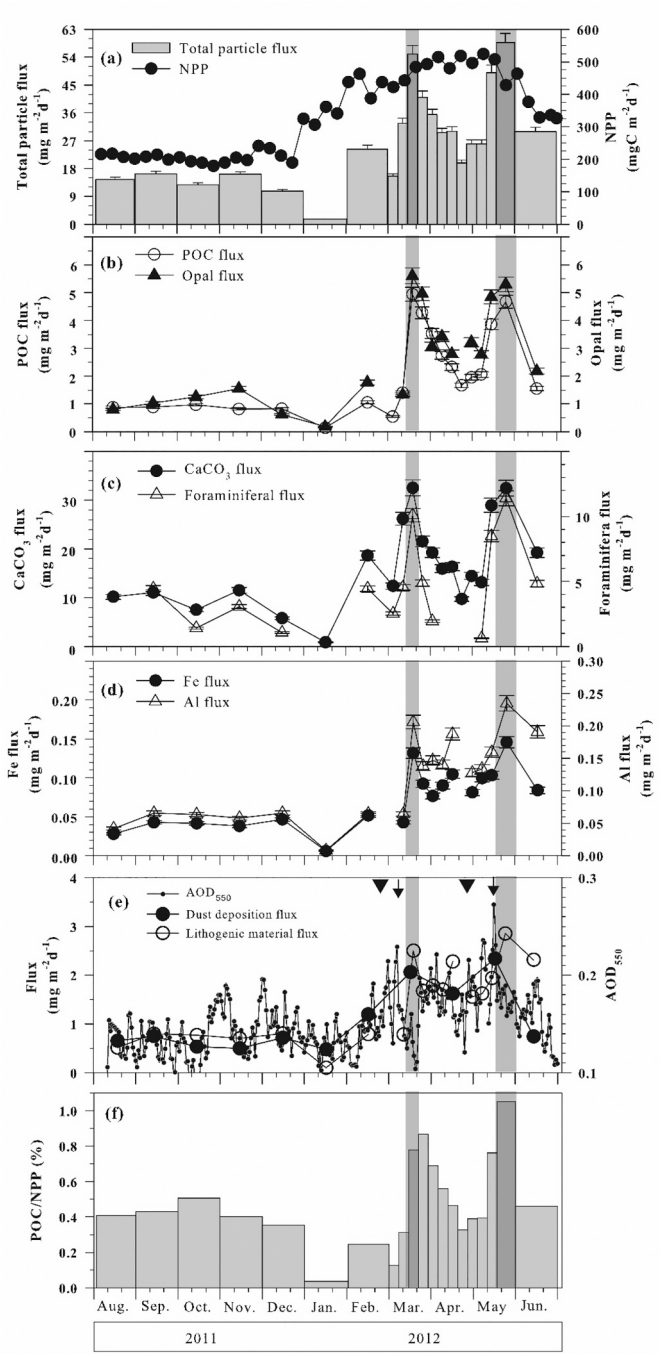

Fig. 3. Temporal variations in the (a) satellite-derived net primary production (NPP) and total particle flux, (b) POC and biogenic opal fluxes, (c) $CaCO_3$ and foraminiferal fluxes, and (d) Al and Fe fluxes at Station KOMO2 from August 2011 to June 2012. (e) Temporal variations in dust deposition to the surface water obtained from the MERRA-2 model, daily MODIS-derived regional mean AOD_{550} (Aerosol Optical Depth at 550 nm) value for the southeastern part of the NPSG, and lithogenic material flux at 4500 m depth, derived from the measured Al concentrations at Station KOMO2. The inverted triangles denote the timing of severe dust events in East Asia (late February and late April 2012), and the arrows highlight the AOD_{550} peaks in March and May 2012. (f) Temporal variations in the ratio of the POC flux at 4500 m depth to the VGPM-based NPP. Missing data are denoted when the lines connecting individual points in the graphs are omitted. The gray shaded regions indicate the two high-particle flux events in spring. The NPP and POC flux are reported in mg C m^{-2} d^{-1}, whereas all of the other flux values are reported in mg m^{-2} d^{-1}. The uncertainties in the fluxes represent 5% of the measured values, a conservative error mainly associated with sample division using a wet sample divider.

opposed to 7-day.

The POC content ranged between 4% and 10%, with an average of 7.2% ± 2.0% (not shown; note that the listed ± values throughout the paper represent the standard deviation of time-series data, not the measurement uncertainty). The mean POC content during the earlier period (August 2011–January 2012) was 6.7% ± 1.3%, and 7.4% ± 2.2% during the later period (February–June 2012), although the difference was not statistically significant. A notable variation was the abrupt increase in POC content from 4.3% to 9% in mid-March, which was accompanied by a sudden increase in POC flux. The seasonal variations in POC flux were generally similar to those in the total particle flux. The POC flux ranged between 0.1 and 4.9 mg m^{-2} d^{-1}, with an average of 2.1 ± 1.5 mg m^{-2} d^{-1} (Fig. 3b). The difference between the earlier and later periods was larger for the POC flux than the total particle flux due to the higher POC content during the later period.

Biogenic opal comprised 8.9% ± 2.4% of the total particulate matter. The biogenic opal flux ranged between 0.18 and 5.6 mg m^{-2} d^{-1}, with an average of 2.6 ± 1.7 mg m^{-2} d^{-1} (Fig. 3b). The temporal variation of biogenic opal flux was remarkably similar to that of the POC flux (R^2 = 0.87, n = 18). The bSi to POC molar ratio ranged between 0.13 and 0.34, with an average of 0.22 ± 0.05; no clear temporal difference was observed in this ratio. $CaCO_3$ comprised 61% ± 10% of the total particulate matter. The temporal variations in $CaCO_3$ flux resembled those of total particulate matter (Fig. 3c). The $CaCO_3$ flux ranged between 0.9 and 32.5 mg m^{-2} d^{-1}, with an average of 16.4 ± 8.6 mg m^{-2} d^{-1}. The flux of planktonic foraminifera, one of the major calcifiers in this region, accounted for 25% ± 8% of the $CaCO_3$ flux (Fig. 3c); the remainder of the $CaCO_3$ flux was presumably from coccolithophores and small foraminiferal fragments. The biogenic opal and $CaCO_3$ fluxes generally exhibited similar temporal variations. The particulate inorganic carbon to POC molar ratio ranged between 0.6 and 2.7, with an average of 1.2 ± 0.6.

Al comprised 0.2%–0.6% of the sinking particulate matter. The Al flux ranged between 0.01 and 0.23 mg m^{-2} d^{-1}, with a duration-weighted average of 0.12 mg m^{-2} d^{-1} (Fig. 3d). Therefore, the lithogenic material (Al × 12.15; Honjo et al., 2000) flux ranged between 0.10 and 2.9 mg m^{-2} d^{-1}, with a duration-weighted average of 1.4 ± 0.8 mg m^{-2} d^{-1} (Fig. 3e). The temporal variations in Al flux were similar to those of POC and opal fluxes. The Al flux exhibited significant positive correlations with the POC (R^2 = 0.69, n = 18), biogenic opal (R^2 = 0.72, n = 18), and $CaCO_3$ (R^2 = 0.55, n = 18) fluxes. Fe accounted for 0.13%–0.43% of the total particulate matter. The Fe flux ranged from 0.006 to 0.15 mg m^{-2} d^{-1}, with a duration-weighted average of 0.07 mg m^{-2} d^{-1} (Fig. 3d). The Fe flux was also closely correlated with the POC (R^2 = 0.78, n = 18) and $CaCO_3$ (R^2 = 0.59, n = 18) fluxes. The Al and Fe fluxes were strongly correlated (R^2 = 0.93, n = 18; not shown). The Fe to Al mass ratio varied between 0.4 and 0.8, with an average of 0.65 ± 0.08 (not shown). Both the biogenic and lithogenic material fluxes were significantly higher in spring 2012 than at other times (ANOVA test for biogenic flux, p = 0.001; for lithogenic material flux, p = 0.003).

4. Discussion

4.1. Primary production and sinking particle flux at depth

A notable observation is that total particle flux was conspicuously higher in March and May 2012. A more general feature in total particle flux is that it was higher from February to June (Fig. 3). The fluxes of the biogenic components all varied in phase with the total particle flux. Biogenic components ($CaCO_3$, biogenic opal, and organic matter) accounted for 85% of sinking particle mass. Current speed measured at 4535 m (35 m below the trap) was mostly 5–10 cm s^{-1} (3.8 ± 2.3 cm s^{-1} on average), below the critical values to affect the sediment trap efficiency (Baker et al., 1988; Honjo et al., 1995) (Fig. S1). No abnormal digression in the current speed and direction was observed during the periods of the two particle flux peaks. Thus, the observed temporal

variation in POC flux is likely the reflection of the temporal variation of phytoplankton production and export in the overlying water column.

Based on the close correlation between NPP and mixed layer depth, the high NPP appears to be caused by nutrient supply by wind-driven deepening of the mixed layer depth. We compared our POC flux results with those at ALOHA site, in the central NPSG, and at KOMO1, which is located further south along the same longitude and mostly affected by the seasonal migration of the ITCZ (Kim et al., 2010, 2011). The range in POC flux at KOMO2 was similar or slightly higher than those at Station ALOHA (2–6 mg C m^{-2} d^{-1} at 4000 m depth, Karl et al., 1996). At ALOHA, two major particle export events, one in February and one in August, were explained by two distinct mechanisms: nitrate supply via upwelling events for the winter pulse and N_2 fixation for the summer pulse (Karl, 1999 and references therein). Our POC flux was more similar to that at KOMO1 in terms of temporal variability (Fig. S2). Similarity between the two sites were also observed in temporal variability in NPP (Fig. S2). Kim et al. (2010, 2011, 2019) reported that the POC flux at KOMO1 was controlled by seasonal deepening of the mixed layer, which in turn was affected mainly by the meridional migration of the Intertropical Convergence Zone (ITCZ). The average POC flux was 4.3 ± 2.3 mg m^{-2} d^{-1} between August 2011 and June 2012, approximately twice the average POC flux at our site (Fig. S2).

The similarity in temporal variability but difference in magnitude in POC flux between KOMO1 and KOMO2 are somewhat expected from the satellite-image of chlorophyll-*a* concentration (Fig. 1). A meridional gradient in chlorophyll-*a* concentration is apparent along the longitude that passes the two sites. Station KOMO2 is located in the southeastern edge of the NPSG, while Station KOMO1 is located in the 10°N thermocline ridge area, representing the region of divergence between the North Equatorial Current (NEC) and North Equatorial Counter Current (NECC). Unlike the equatorial Pacific region, the 10°N thermocline ridge area showed distinct seasonal changes arising from seasonal shift of the ITCZ that influence the local upwelling and particle flux (Kim et al., 2011). In addition to the seasonal variability, the El Niño Southern Oscillation (ENSO) produces interannual variation of particle flux in the eastern tropical Pacific (e.g., Dymond and Collier, 1988; Honjo et al., 1995; Kim et al., 2011, 2019). A La Niña condition lasted for almost 10 months from July 2011 to April 2012, which may have enhanced the NPP and POC flux at both sites.

Biological production in the surface water and sinking particle flux at 4500 m depth are loosely coupled in a seasonal sense. However, the two biogenic material peaks and low values between these peaks were not observed in the NPP time series. Surprisingly, POC flux in May at KOMO2 was even higher than at KOMO1 (Fig. S2). The abrupt peak in POC flux in March 2012 was accompanied by an abrupt increase in POC content, implying the rapid vertical transport of biogenic material to the 4500 m sampling depth (Grabowski et al., 2019). The lithogenic material fluxes were also highest during the two particle flux peaks, thus implying a potential role of lithogenic material in enhancing particle flux. We therefore investigated the influence of aeolian dust deposition on biogenic particle flux in the following section.

4.2. Atmospheric dust deposition and its influence on the biological pump

An annual average atmospheric dust deposition of 1.1 mg m^{-2} d^{-1} was derived from the MERRA-2 model, with this relatively low value being comparable to previously reported values for the NPSG (0.5–1.4 mg m^{-2} d^{-1}, Jickells et al., 2005; Duce, 2014). Atmospheric dust deposition was notably higher in March–May 2012 (Fig. 3e). The precipitation was generally low in March–May 2012 and thus the dust deposition was mainly through dry deposition (precipitation data were obtained from Tropical Rainfall Measuring Mission; http://giovanni.gsfc.nasa.gov). Severe dust events in East Asia occurred from late February to late April 2012 (Kanatani et al., 2014; Lee et al., 2015; Yu et al., 2016). The NASA MODIS satellite aerosol sensor observed high AOD values around the study region during 1–7 March and 7–16 May 2012 (Fig. 3e). Backward trajectory analysis based on the NOAA HYSPLIT model (available at http://ready.arl.noaa.gov) showed that the prominent dust deposition events in early March and May originated from northern China and Mongolia (Fig. 4). The lithogenic material flux, derived from the Al flux, showed two peaks during 15–21 March and 17–31 May 2012. Time lags of about 2 weeks were observed between the AOD and lithogenic material flux peaks (Fig. 3e). There were remarkable similarities in both the temporal variability and magnitude between the dust deposition to the surface water and lithogenic material flux at 4500 m depth during the study period (Fig. 3e). Therefore, we consider that EAD deposition was the main source of lithogenic material at depth. These observations imply that the dust has a very short residence time in the water column, which was also shown for Station ALOHA (Letelier et al., 2019) and subtropical oligotrophic sites in the North Atlantic (e.g., Neuer et al., 2004; Brust et al., 2011).

Martino et al. (2014) demonstrated that nutrient supply via dust deposition sustains ~10% of the primary production at Station ALOHA. If the same is true for our site, then it is unlikely that dust deposition is the main enhancer of primary productivity at the study site. A more conspicuous effect of dust deposition may be the enhanced export and transfer efficiency of biogenic particles. The influence of dust deposition on the biological pump efficiency is reflected in the ratio of the POC flux at 4500 m depth to the NPP from the surface ocean. The efficiency includes both the export of POC from the bottom of the mixed layer and transport to the sampling depth in this case. This ratio ranged between 0.13% and 1.1%, except for the anomalously low particle flux observation in January 2012 (Fig. 3f). The ratio for March–May (0.6% ± 0.23%) was about twice the value for the rest of the study period (0.35% ± 0.14%), indicating effective carbon sequestration in this period. The difference in POC flux to NPP ratio between the two peaks (March and May 2012) and the rest of the study periods was statistically significant (ANOVA, $p = 0.029$). The highest values (0.9%–1.1%) were observed for the two atmospheric dust deposition events, implying that dust deposition played an important role in transporting the produced biogenic particles into the deep-sea (Fig. 3f). However, exact mechanisms are not clear. Lithogenic material content was not exceedingly high for enhanced ballasting. Lithogenic particles may have acted as nuclei for flocculation of biogenic particles. The ratio of the POC to the sum of $CaCO_3$ and biogenic opal was notably higher in March–May (average = 0.13) than in the rest of the study period (0.08) (ANOVA, $p = 0.03$). The high ratio might have also been caused by the enhanced preservation of organic matter due to the rapid sinking of organic particles (Grabowski et al., 2019).

Pabortsava et al. (2017) reported that dust deposition in the subtropical North Atlantic resulted in higher N_2 fixation and primary production by *Trichodesmium* species. This resulted in a doubling of the sinking POC flux, whereas the biogenic opal flux did not exhibit a significant difference between the dust-rich and dust-poor regions (Pabortsava et al., 2017). The enhanced POC and biogenic opal fluxes during the dust deposition events can be at least partly attributed to diatom blooms at our site. The plankton bloom in the NPSG is typically dominated by large diatoms (Dore et al., 2008), the growth of which is limited primarily by the availability of Fe and nitrate (DiTullio et al., 1993; Rafter et al., 2017). Input of Fe via EAD may have stimulated the diatom blooms and POC export. The contribution of biogenic opal to the total particle flux increased from 7.5% to 10% during the dust deposition period (March–May), although this difference was not statistically significant. In addition to the primary producer, the planktonic foraminiferal flux also showed a marked increase during the dust deposition period. Planktonic foraminiferal flux is closely related to the variation of phytoplankton biomass (Kim et al., 2010) and may have helped particle export. The multiple linear regression analysis of POC flux with those of biogenic opal, $CaCO_3$, and lithogenic material (Honda and Watanabe, 2010; Le Moigne et al., 2012) showed that POC flux could be well explained by biogenic opal flux with the carrying coefficient of 0.92 (i.e., 92% contribution to the total POC flux). However, POC flux was not

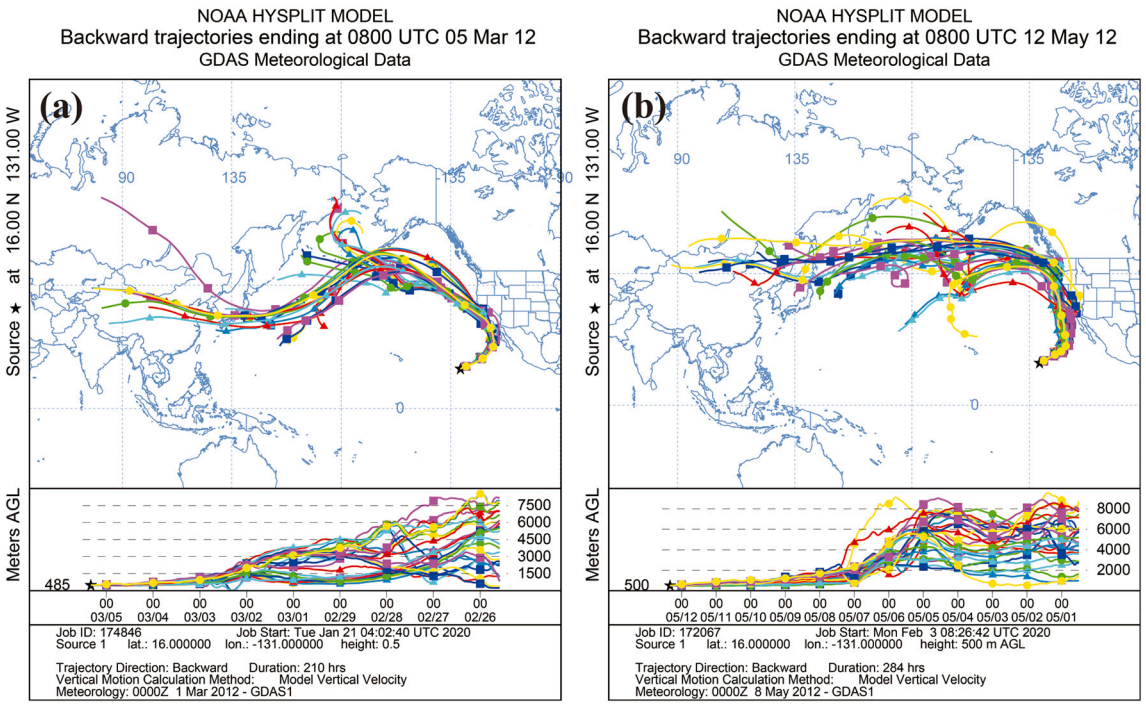

Fig. 4. Backward atmospheric particle ensemble trajectories at Station KOMO2 in the NPSG for 26 February–5 March (a) and 1–12 May 2012 (b). The backward trajectory data are based on the NOAA HYSPLIT model (http://ready.arl.noaa.gov).

significantly correlated with either $CaCO_3$ flux or lithogenic material flux ($p > 0.4$). Thus, the ballast effect of $CaCO_3$ and lithogenic material was not significant.

Although the role of dust deposition in enhancing POC flux is apparent, it is hard to deconvolute the effect of nutrient supply via dust deposition from that via water column mixing based on our results alone, because both occur in the same seasons. We attempted to estimate the contribution of dust deposition to NPP following Neuer et al. (2004). The effect of the Fe-derived from dust deposition was estimated under the assumption that ~3.5% of dust was Fe, ~10% of the dust-derived Fe was soluble (Zhuang et al., 1990; Fung et al., 2000; Neuer et al., 2004), and the POC/Fe molar ratio in phytoplankton was 100,000 (Coale et al., 1996; Neuer et al., 2004). Monthly Fe deposition ranged between 0.02 and 0.08 mg $m^{-2}d^{-1}$ (0.037 ± 0.02 mg $m^{-2}d^{-1}$ = 13.5 mg m^{-2} yr^{-1} on average), which is comparable to the annual flux of atmospheric Fe into the North Pacific Subtropical gyre estimated by Duce and Tindale (1991), 10 mg m^{-2} yr^{-1}. The dust-derived Fe would account for 23 ± 7% of the annual NPP. This value increases to 44 ± 11% in March–May 2012: for this estimate, we used the observed Fe flux at 4500 m for dust deposition because of the lack of high-resolution atmospheric dust input data. In contrast to Fe, under the assumption of total nitrogen content of 0.05% in the dust (Neuer et al., 2004), the maximum N-input by dust was up to 0.0012 mg $m^{-2}d^{-1}$, only ~0.25% of particulate N flux at 4500 m. Using the C/N molar ratio of 106/16, contribution to NPP by the N-input was <0.001% of the NPP. Thus, it is not clear how the dust deposition enhanced the export efficiency because dust-derived N input was negligible. The additional supply of Fe and other nutrients may have affected the phytoplankton community structure. For example, changing the silicifiers species may affect the sinking rate and export efficiency. In this sense, planktonic community need to be investigated together with the particle fluxes in the future.

Our results have some similarities and dissimilarities to the results at Station ESTOC in the eastern subtropical North Atlantic gyre, where the atmospheric dust deposition was about one order of magnitude higher than at our study site (Neuer et al., 2004). At both sites, dust deposition was not accompanied by enhanced NPP and atmospheric N supply was not considerable. However, dust-derived Fe could satisfy considerable portions of Fe demand by phytoplankton at both sites and may hold the key for the enhanced particle flux, which needs further study. Also, the role of lithogenic material as ballasting agent was less important than biogenic minerals. However, biogenic opal was the major ballasting mineral at our site, whereas it was $CaCO_3$ (e.g., coccolithophorids) at Station ESTOC. Careful examination of the dust deposition, lithogenic material flux, and NPP for a more extended period will be necessary to better understand the influence of dust deposition on the biological pump in the oligotrophic subtropical gyres.

5. Summary and implications

We investigated the particulate matter flux to 4500 m for about a year in the southeastern edge of the NPSG, with an increase in particulate matter flux observed during the March–May period. This period generally coincided with the high NPP period. The biogenic opal content was also high during this period, indicating the importance of diatom blooms in particulate fluxes to the deep ocean. Two peaks in the particulate matter flux in March and May 2012 coincided with atmospheric dust deposition events. The remarkable similarity, both in magnitude and temporal variability, between dust deposition and the lithogenic material flux suggests a strong coupling between these two processes. The POC transfer efficiency to the ocean interior was the highest during these peak flux periods. Diatom blooms stimulated by dust deposition were the likely cause of this efficient POC transport to the deep ocean.

EAD deposition in the North Pacific has been decreasing in recent decades due to increasing vegetation cover in the source regions (Wang et al., 2008; Che et al., 2015; An et al., 2018). There has been a significant decrease in the outbreaks of severe EAD events in the northern China and Mongolia deserts since 2011 (Che et al., 2015; An et al., 2018). Attention should therefore be directed to the recent downturn in spring EAD events, which may affect the biological pump efficiency and ultimately sea-to-air CO_2 exchange in the NPSG.

Declaration of Competing Interest

The authors declare that they have no known competing financial

interests or personal relationships that could have appeared to influence the work reported in this paper.

Acknowledgements

This work was supported by the Korean Government's Ministry of Oceans and Fisheries R&D grant (PM61701) and KIOST grant PE99923 and PE99912, south Korea.

Appendix A. Supplementary data

Supplementary data to this article can be found online at https://doi.org/10.1016/j.jmarsys.2021.103634.

References

Acker, J.G., Leptoukh, G., 2007. Online analysis enhances use of NASA Earth science data. EOS Trans. Am. Geophys. Union 88 (2), 14–17. https://doi.org/10.1029/2007eo020003.

An, L., Che, H., Xue, M., Zhang, T., Wang, H., Wang, Y., Zhou, C., Zhao, H., Gui, K., Zheng, Y., Sun, T., Liang, Y., Sun, E., Zhang, H., Zhang, X., 2018. Temporal and spatial variations in sand and dust storm events in East Asia from 2007 to 2016: relationships with surface conditions and climate change. Sci. Total Environ. 633, 452–462. https://doi.org/10.1016/j.scitotenv.2018.03.068.

Baker, E.T., Milburn, H.B., Tennant, D.A., 1988. Field assessment of sediment trap efficiency under varying flow condition. J. Mar. Syst. 46, 573–592.

Behrenfeld, M.J., Falkowski, P.G., 1997. Photosynthetic rates derived from satellite-based chlorophyll concentration. Limnol. Oceanogr. 42 (1), 1–20. https://doi.org/10.4319/lo.1997.42.1.0001.

Behringer, D.W., Xue, Y., 2004. Evaluation of the global ocean data assimilation system at NCEP: the Pacific Ocean. In: Eight Symposium on Integrated Observing and Assimilation Systems for Atmosphere, Oceans, and Land Surface, AMS 84th Annual Meeting, Washington State Convention and Trade Center, Seattle, Washington, 11-15.

Behringer, D.W., Ji, M., Leetmaa, A., 1998. An improved coupled model for ENSO prediction and implications for ocean initialization. Part I: The ocean data assimilation system. Mon. Weather Rev. 126, 1013–1021.

Bishop, J.K.B., Davis, R.E., Sherman, J.T., 2002. Robotic observations of dust storm enhancement of carbon biomass in the North Pacific. Science 298 (5594), 817–821. https://doi.org/10.1126/science.1074961.

Brust, J., Waniek, J.J., 2010. Atmospheric dust contribution to deep-sea particle fluxes in the subtropical Northeast Atlantic. Deep-Sea Res. Part I: Oceanogr. Res. Pap. 57, 988–998.

Brust, J., Schulz-Bull, D.E., Leipe, T., Chavagnac, V., Waniek, J.J., 2011. Descending particles: from the atmosphere to the deep ocean-a time series study in the subtropical NE Atlantic. Geophys. Res. Lett. 38, L06603 https://doi.org/10.1029/2010GL045399.

Calil, P.H.R., Doney, S.C., Yumimoto, K., Eguchi, K., Takemura, T., 2011. Episodic upwelling and dust deposition as bloom triggers in low-nutrient, low-chlorophyll regions. J. Geophys. Res. Oceans 116 (C6), C06030. https://doi.org/10.1029/2010jc006704.

Che, H., Zhao, H., Wu, Y., Xia, X., Zhu, J., Dubovik, O., Estelles, V., Ma, Y., Wang, Y., Wang, H., Wang, Y., Zhang, X., Shi, G., 2015. Application of aerosol optical properties to estimate aerosol type from ground-based remote sensing observation at urban area of northeastern China. J. Atmos. Sol. Terr. Phys. 132, 37–47. https://doi.org/10.1016/j.jastp.2015.06.015.

Coale, K.H., Johnson, K.S., Fitzwater, S.E., Gordon, R.M., Tanner, S., Chavez, F.P., et al., 1996. A masive phytoplankton bloom induced by an ecosystem-scale iron fertilization experiment in the equatorial Pacific Ocean. Nature 383, 495–501.

DiTullio, G.R., Hutchins, D.A., Bruland, K.W., 1993. Interaction of iron and major nutrients controls phytoplankton growth and species composition in the tropical North Pacific Ocean. Limnol. Oceanogr. 38 (3), 495–508. https://doi.org/10.4319/lo.1993.38.3.0495.

Dore, J.E., Letelier, R.M., Church, M.J., Lukas, R., Karl, D.M., 2008. Summer phytoplankton blooms in the oligotrophic North Pacific subtropical gyre: historical perspective and recent observations. Prog. Oceanogr. 76 (1), 2–38. https://doi.org/10.1016/j.pocean.2007.10.002.

Duce, R.A., 2014. A dusty planet. Oceanography 27 (1), 66–68.

Duce, R.A., Tindale, N.W., 1991. Atmospheric transport of iron and its deposition in the ocean. Limnol. Oceanpgraphy 36 (8), 1715–1726.

Dymond, J., Collier, R., 1988. Biogenic particle fluxes in the equatorial pacific: evidence for both high and low productivity during the 1982-1983 El Niño. Glob. Biogeochem. Cycles 2, 129–137.

Fung, L., Meyn, S., Tegen, I., Doney, S.C., John, J., Bishop, J.K.B., 2000. Iron supply and demand in the upper ocean. Glob. Biogeochem. Cycles 14, 281–296.

German, C.R., Colley, S., Palmer, M.R., Khripounoff, A., Klinkhammer, G.P., 2002. Hydrothermal plume-particle fluxes at 13°N on the East Pacific Rise. Deep-Sea Res. Part I: Oceanogr. Res. Pap. 49 (11), 1921–1940. https://doi.org/10.1016/S0967-0637(02)00086-9.

Grabowski, E., Letelier, R.M., Laws, E.A., Karl, D.M., 2019. Coupling carbon and energy fluxes in the North Pacific Subtropical Gyre. Nat. Commun. 10, 1895. https://doi.org/10.1038/s41467-019-09772-z.

Harrison, P.J., Boyd, P.W., Varela, D.E., Takeda, S., Shiomoto, A., Odate, T., 1999. Comparison of factors controlling phytoplankton productivity in the NE and NW subarctic Pacific gyres. Prog. Oceanogr. 43 (2), 205–234. https://doi.org/10.1016/S0079-6611(99)00015-4.

Honda, M.C., Watanabe, S., 2010. Importance of biogenic opal as ballast of particulate organic carbon (POC) transport and existence of mineral ballast-associated and residual POC in the Western Pacific Subarctic Gyre. Geophys. Res. Lett. 37 (2), L02605 https://doi.org/10.1029/2009GL041521.

Honjo, S., Manganini, S.J., 1993. Annual biogenic particle fluxes to the interior of the North Atlantic Ocean: studied at 34°N 21°W and 48°N 21°W. Deep-Sea Res. I 47, 587–607.

Honjo, S., Dymond, J., Collier, R., Manganini, S.J., 1995. Export production of particles to the interior of the equatorial Pacific Ocean during the 1992 EqPac experiment. Deep-Sea Res. II 42, 831–870.

Honjo, S., Francois, R., Manganini, S., Dymond, J., Collier, R., 2000. Particle fluxes to the interior of the Southern Ocean in the Western Pacific sector along 170°W. Deep-Sea Res. Part II: Top. Stud. Oceanogr. 47 (15), 3521–3548. https://doi.org/10.1016/S0967-0645(00)00077-1.

Jickells, T.D., An, Z.S., Andersen, K.K., Baker, A.R., Bergametti, G., Brooks, N., Cao, J.J., Boyd, P.W., Duce, R.A., Hunter, K.A., Kawahata, H., Kubilay, N., LaRoche, J., Liss, P. S., Mohowald, N., Prospero, J.M., Ridgwell, A.J., Tegen, I., Torres, R., 2005. Global iron connections between desert dust, ocean biogeochemistry, and climate. Science 308 (5718), 67–71. https://doi.org/10.1126/science.1105959.

Johnson, K.S., Elrod, V.A., Fitzwater, S.E., Plant, J.N., Chavez, F.P., Tanner, S.J., Gordon, R.M., Westphal, D.L., Perry, K.D., Wu, J., Karl, D.M., 2003. Surface Ocean-lower atmosphere interactions in the Northeast Pacific Ocean gyre: aerosols, iron, and the ecosystem response. Glob. Biogeochem. Cycles 17 (2), 1063. https://doi.org/10.1029/2002gb002004.

Kanamitsu, M., Ebisuzaki, W., Woollen, J., Yang, S.K., Hnilo, J.J., Fiorino, M., Potter, G. L., 2002. NCEP-DOE AMIP-II reanalysis (R-2). Bull. Am. Meteorol. Soc. 83, 1631–1643.

Kanatani, K.T., Okumura, M., Tohno, S., Adachi, Y., Sato, K., Nakayama, T., 2014. Indoor particle counts during Asian dust events under everyday conditions at an apartment in Japan. Environ. Health Prev. Med. 19 (1), 81–88. https://doi.org/10.1007/s12199-013-0356-4.

Karl, D.M., 1999. A sea of change: biogeochemical variability in the North Pacific Subtropical Gyre. Ecosystems 2 (3), 181–214. https://doi.org/10.1007/s100219900068.

Karl, D.M., Church, M.J., 2017. Ecosystem structure and dynamics in the North Pacific Subtropical Gyre: new views of an old ocean. Ecosystems 20 (3), 433–457.

Karl, D.M., Letelier, R.M., 2008. Nitrogen fixation-enhanced carbon sequestration in low nitrate, low chlorophyll seascapes. Mar. Ecol. Prog. Ser. 364, 257–268.

Karl, D.M., Christian, J.R., Dore, J.E., Hebel, D.V., Letelier, R.M., Tupas, L.M., Winn, C. D., 1996. Seasonal and interannual variability in primary production and particle flux at Station ALOHA. Deep-Sea Res. Part II: Top. Stud. Oceanogr. 43, 539–568.

Kim, H.J., Hyeong, K., Yoo, C.M., Chi, S.B., Khim, B.K., Kim, D., 2010. Seasonal variations of particle fluxes in the northeastern equatorial Pacific during normal and weak El Niño periods. Geosciences 14 (4), 415–422.

Kim, H.J., Kim, D., Yoo, C.M., Chi, S.B., Khim, B.K., Shin, H.R., Hyeong, K., 2011. Influence of ENSO variability on sinking-particle fluxes in the northeastern equatorial Pacific. Deep-Sea Res. Part I-Oceanogr. Res. Pap. 58 (8), 865–874. https://doi.org/10.1016/j.dsr.2011.06.007.

Kim, H.J., Hyeong, K., Yoo, C.M., Khim, B.K., Kim, K.H., Son, J.W., Kug, J.S., Park, J.Y., Kim, D., 2012. Impact of strong El Niño events (1997/98 and 2009/10) on sinking particle fluxes in the 10°N thermocline ridge area of the northeastern equatorial Pacific. Deep-Sea Res. Part I: Oceanogr. Res. Pap. 67, 111–120. https://doi.org/10.1016/j.dsr.2012.05.008.

Kim, H.J., Kim, T.W., Hyeong, K., Yeh, S.W., Park, J.Y., Yoo, C.M., Hwang, J., 2019. Suppressed CO_2 outgassing by an enhanced biological pump in the Eastern Tropical Pacific. J. Geophys. Res. Oceans 124, 7962–7973. https://doi.org/10.1029/2019JC015287.

Le Moigne, F.A.C., Sanders, R.J., Villa-Alfageme, M., Martin, A.P., Pabortsava, K., Planquette, H., Morris, P.J., Thomalla, S.J., 2012. On the proportion of ballast versus non-ballast associated carbon export in the surface ocean. Geophys. Res. Lett. 37, L15610 https://doi.org/10.1029/GL052980.

Lee, K.E., Bahk, J.J., Narita, H., 2003. Temporal variations in productivity and planktonic ecological structure in the East Sea (Japan Sea) since the last glaciation. Geo-Mar. Lett. 23 (2), 125–129. https://doi.org/10.1007/s00367-003-0132-3.

Lee, Y.G., Ho, C.-H., Kim, J.-H., Kim, J., 2015. Quiescence of Asian dust events in South Korea and Japan during 2012 spring: dust outbreaks and transports. Atmos. Environ. 114, 92–101. https://doi.org/10.1016/j.atmosenv.2015.05.035.

Letelier, R.M., Björkman, K.M., Church, M.J., Hamilton, D.S., Mahowald, N.M., Scanza, R.A., Schneider, N., White, A.E., Karl, D.M., 2019. Climate-driven oscillation of phosphorous and iron limitation in the North Pacific Subtropical Gyre. Proc. Nat. Acad. Sci. U. S. Am. 116 (26), 12720–12728. https://doi.org/10.1073/pnas.1900789116.

Li, T., Masuzawa, T., Kitagawa, H., 2004. Seasonal variations in settling fluxes of major components in the oligotrophic Shikoku Basin, the western North Pacific: coincidence of high biogenic flux with Asian dust supply in spring. Mar. Chem. 91 (1), 187–210. https://doi.org/10.1016/j.marchem.2004.06.010.

Martino, M., Hamilton, D., Baker, A.R., Jickells, T.D., Bromlry, T., Nojiri, Y., Quack, B., Boyd, P.W., 2014. Western Pacific atmospheric nutrient deposition fluxes, their

impact on surface ocean productivity. Glob. Biogeochem. Cycles 28 (7), 712–728. https://doi.org/10.1002/2013GB004794.
Mortlock, R.A., Froelich, P.N., 1989. A simple method for the rapid determination of biogenic opal in pelagic marine sediments. Deep-Sea Res. Part A. Oceanogr. Res. Pap. 36 (9), 1415–1426. https://doi.org/10.1016/0198-0149(89)90092-7.
Müller, P.J., Schneider, R., 1993. An automated leaching method for the determination of opal in sediments and particulate matter. Deep-Sea Res. Part I: Oceanogr. Res. Pap. 40 (3), 425–444. https://doi.org/10.1016/0967-0637(93)90140-X.
Neuer, S., Torres-Padron, M.E., Gelado-Caballero, M.D., Rueda, M.J., Hernandez-Brito, J., Davenport, R., Wefer, G., 2004. Dust deposition pulses to the eastern subtropical North Atlantic gyre: does ocean's biogeochemistry respond? Golal Biogeochem. Cycles 18, GB4020. https://doi.org/10.1029/2004GB002228.
Pabortsava, K., Lampitt, R.S., Benson, J., Crowe, C., McLachlan, R., Moigne, Le, Moore, C.M., Pebody, C., Provost, P., Rees, A.P., Tilstone, G.H., Woodward, E.M.S., 2017. Carbon sequestration in the deep Atlantic enhanced by Saharan dust. Nat. Geosci. 10, 189. https://doi.org/10.1038/ngeo2899.
Papadimas, C.D., Hatzianastassiou, N., Mihalopoulos, N., Kanakidou, M., Katsoulis, B.D., Vardavas, I., 2009. Assessment of the MODIS collections C005 and C004 aerosol optical depth products over the Mediterranean basin. Atmos. Chem. Phys. 9 (9), 2987–2999. https://doi.org/10.5194/acp-9-2987-2009.
Rafter, P.A., Sigman, D.M., Mackey, K.R.M., 2017. Recycled iron fuels new production in the eastern equatorial Pacific Ocean. Nat. Commun. 8 (1), 1100. https://doi.org/10.1038/s41467-017-01219-7.
Randle, C.A., da Silva, A.M., Buchard, V., Colarco, P.R., Darmenov, A., Govindaraju, R., Smirnov, A., Holben, B., Ferrare, R., Hair, J., Shinozuka, Y., Flynn, C.J., 2017. The MERRA-2 aerosol reanalysis, 1980 – onward. Part I: system description and data assimilation evaluation. J. Clim. 30, 6823–6850.
Reynolds, R.W., Rayner, N.A., Smith, T.M., Stokes, D.C., Wang, W., 2002. An improved in situ and satellite SST analysis for climate. J. Clim. 15, 1609–1625.
Seo, I., Lee, Y.I., Yoo, C.M., Kim, H.J., Hyeong, K., 2014. Sr-Nd isotope composition and clay mineral assemblages in eolian dust from the central Philippine Sea over the last 600 kyr: implications for the transport mechanism of Asian dust. J. Geophys. Res. Atmos. 119 (19), 11492–11504. https://doi.org/10.1002/2014jd022025.
Tan, S.-C., Yao, X., Gao, H.-W., Shi, G.-Y., Yue, X., 2013. Variability in the correlation between Asian dust storms and chlorophyll a concentration from the North to Equatorial Pacific. PLoS One 8 (2), e57656. https://doi.org/10.1371/journal.pone.0057656.
Trapote, M.C., Vegas-Vilarrúbia, T., López, P., Puche, E., Gomà, J., Buchaca, T., Canellas-Bolta, N., Safont, E., Corella, J.P., Rull, V., 2018. Modern sedimentary analogues and integrated monitoring to understand varve formation in the Mediterranean Lake Montcortès (Central Pyrenees, Spain). Palaeogeogr. Palaeoclimatol. Palaeoecol. 496, 292–304. https://doi.org/10.1016/j.palaeo.2018.01.046.
Wang, X., Huang, J., Ji, M., Hiquchi, K., 2008. Variability of East Asia dust events and their long-term trend. Atmos. Environ. 42, 3156–3165.
White, A.E., Spitz, Y.H., Letelier, R.M., 2007. What factors are driving summer phytoplankton blooms in the North Pacific subtropical gyre? J. Geophys. Res. Oceans 112 (C12), C12006. https://doi.org/10.1029/2007jc004129.
Yoon, J.-E., Kim, K., Macdonald, A.M., Park, K.-T., Kim, H.-C., Yoo, K.-C., Yoon, H.I., Yang, E.J., Jung, J., Lim, J.H., Kim, J.H., Lee, J., Choi, T.J., Song, J.M., Kim, I.N., 2017. Spatial and temporal variabilities of spring Asian dust events and their impacts on chlorophyll-a concentrations in the western North Pacific Ocean. Geophys. Res. Lett. 44 (3), 1474–1482. https://doi.org/10.1002/2016gl072124.
Yu, X., Lü, R., Kumar, K.R., Ma, J., Zhang, Q., Jiang, Y., Kang, N., Yang, S., Wang, J., Li, M., 2016. Dust aerosol properties and radiative forcing observed in spring during 2001–2014 over urban Beijing, China. Environ. Sci. Pollut. Res. 23 (15), 15432–15442. https://doi.org/10.1007/s11356-016-6727-9.
Yuan, W., Zhang, J., 2006. High correlations between Asian dust events and biological productivity in the western North Pacific. Geophys. Res. Lett. 33 (7), L07603 https://doi.org/10.1029/2005gl025174.
Zhuang, G., Duce, R.A., Kester, D.R., 1990. The dissolution of atmospheric iron in the surface seawater of the open ocean. J. Geophys. Res. 95, 16207–16216.